PROCEEDINGS, Thirty-Seventh Workshop on Geothermal Reservoir Engineering
Stanford University, Stanford, California, January 30 - February 1, 2012
SGP-TR-194

BOREHOLE IMAGE LOG AND STATISTICAL ANALYSIS OF FOH-3D, FALLON NAVAL AIR STATION, NV

Kelly Blake[1, 2] and Nicholas C. Davatzes[2]

[1]Naval Geothermal Program Office, China Lake, CA 93555

[2] Earth and Environmental Science Temple University, Philadelphia, PA 19122

e-mail: kelly.blake@navy.mil and davatzes@temple.edu

ABSTRACT

Formation Micro-Scanner (FMS) and Acoustic Borehole Televiewer (BHTV) image logs from borehole FOH-3D in the volcanic and metavolcanic rock of the Fallon Naval Air Station, NV were analyzed to identify natural fractures and constrain the stress field acting on the fractures proximal to the borehole and to the geothermal system. Abundant natural fractures are revealed in these logs, defining two conjugate fracture sets, which strikes ~010° and dips at ~58° to the E and W respectively. The average azimuth of S_{hmin} ± one standard deviation revealed by extensive borehole wall breakouts and tensile fractures, as well as petal-centerline fractures, is 097±12° for the near vertical portion of the borehole. Spectral analysis of the depth variation of the horizontal principal stress azimuth revealed in the BHTV image indicates that rotations of these stress components about the vertical axis yield a linear spectral slope of -3.03±0.2 log (deg^2*m)(m) in a frequency range of from $10^{-2.4}$ to $10^{-1.35}$ m^{-1}. This spectral slope is consistent with a stable, fractal dependence of stress rotations on length-scale and characterizes the inherent heterogeneity of the principal stress directions in the volume traversed by the borehole.

Together, the organization of the fracture population into conjugate sets and an azimuth of S_{Hmax} consistently parallel to the strike of the conjugate set indicate that these fractures are well oriented for normal slip. The natural fractures have similar orientations to the Stillwater Range Front Fault proximal to the borehole, as well as numerous seismogenic faults west of the Stillwater Range in the Carson Basin. This azimuth of S_{hmin} is similar to the regional S_{hmin} azimuths for the normal faulting in the Basin and Range province and to previous stress orientation analyses of borehole-induced structures at Dixie Valley, Desert Peak, and Brady's geothermal systems.

INTRODUCTION

Principal stress orientations in the Basin and Range acquired through focal mechanisms, image log analysis (e.g., World Stress Map, 2008; Heidbach et al., 2010), in-situ stress measurements (e.g., Hickman et al., 2002; Davatzes and Hickman, 2009), fault slip data (Belier and Zoback, 1995), alignments of volcanic structures (Zoback, 1989), as well as geodetic measurements of strain (Bennett et al., 2003; Hammond and Thatcher, 2005; Kremer et al., 2009; 2010) all demonstrate variation in stress orientation at a variety of length-scales (Figure 1) (Zoback, 1989). Variations in principal stress orientation are visible at the one to hundreds of kilometer length scales in Figure 1, but these variations also occur throughout the depth of the brittle crust on the centimeter to meter scale (Day-Lewis et al, 2010; Valley and Evans, 2011; Blake and Davatzes, 2011). In geothermal reservoirs the stress state related to development and maintenance of the geothermal system is of interest for discovering geothermal fields (Curewitz and Karson, 1997; Davatzes and Hickman, 2006; Faulds et al., 2006), for locating wells because of the impact of stress on borehole stability and fracture permeability (e.g., Barton et al., 1995; Heffer, 2002), and predicting the reservoir response to pressure changes resulting from production injection (Heffer, 2002). In particular, Heffer (2002) shows that the stress direction in combination with fracture sets tends to reveal the direction of greatest permeability in reservoirs, even in systems thought not be fracture dominated. In enhanced geothermal systems (EGS), stress and its heterogeneity is a key control on the potential of fractures to interact with hydraulic stimulation, constrains the direction the stimulation is likely to grow (e.g., Rutledge et al.,

2003), and constrains the seismic risk associated with inducing earthquakes on large faults of known orientation (Majer et al., 2007).

In this study both Formation Micro-Scanner (FMS) and ABI85 Acoustic Borehole (BHTV) image logs from the FOH-3D borehole on the Fallon Naval Air Station, Nevada are used to constrain the stress state and natural fracture population proximal to the borehole as part of characterizing this geothermal prospect. The abundant drilling-induced structures are used to infer the regional azimuth of the maximum horizontal compressive stress, S_{Hmax}, and length-scale dependent heterogeneity in the horizontal principal stress azimuth along the path of the FOH-3D borehole.

a)

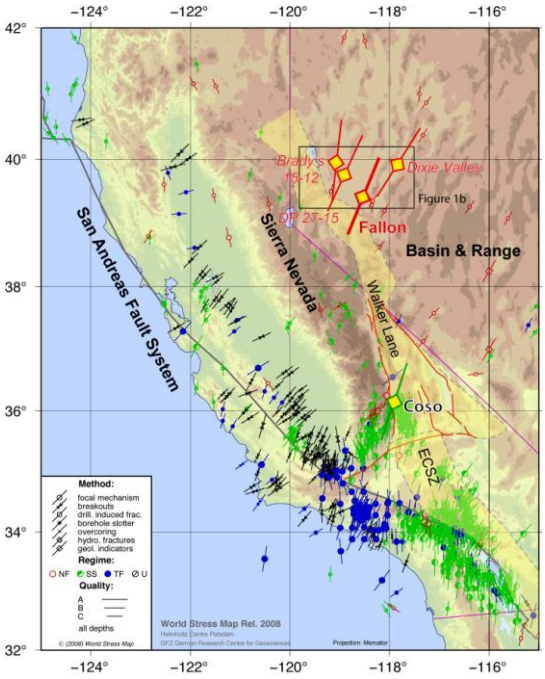

b)

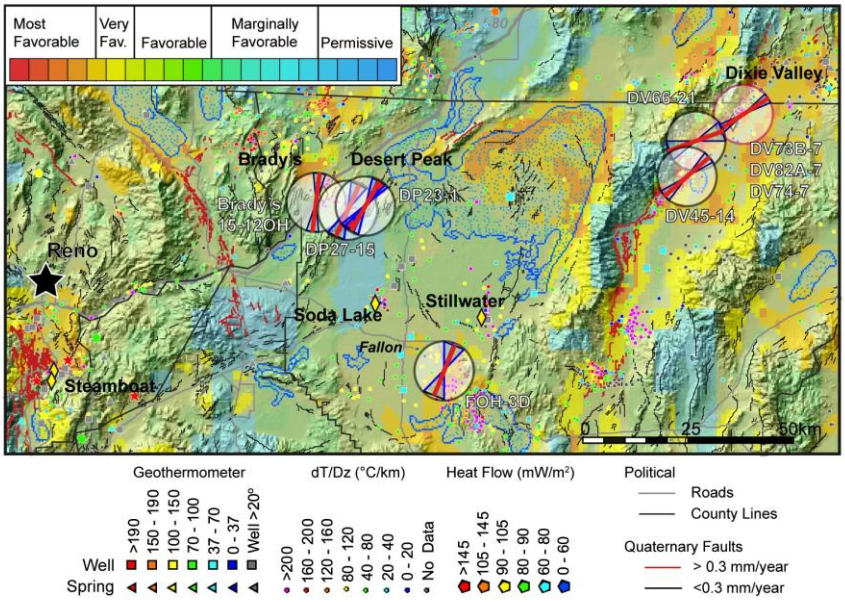

Figure 1: a) S_{Hmax} orientations and tectonic setting (modified from the World Stress Map, 2008). Data is plotted for all depth ranges. Larger, labeled symbols represent average stresses typically from multiple wells in nearby geothermal fields: Coso (Davatzes and Hickman, 2010; Blake and Davatzes, 2011); Desert Peak, wells 23-1 (Robertson-Tait et al.; 2004) and DP 27-15 (Davatzes and Hickman, 2009; Hickman and Davatzes, 2010); Brady's (Moos et al., unpublished data); and Dixie Valley (Barton et al., 1998; Hickman et al., 2000 and references therein); Fallon (this paper). Region of enhanced extension is inferred from Zoback (1989), Bellier and Zoback (1995), Faulds et al. (2006); Kreemer et al. (2009); Thatcher et al. (1999; 2005); and geothermal potential quaternary fault activity is from Coolbaugh et al. (2005) and Thatcher et al. (1999). b) The black box is enlarged from 1a to show the variation in S_{Hmax} throughout this area of the Basin and Range.

GEOLOGIC SETTING

Fallon is located in Nevada along the western edge of the Basin and Range Province and near the northern terminus of the Eastern California Shear Zone an area associated with normal faulting, thinning of the brittle crust and high heat flow (Hill, 1971; Eaton, 1982) where the majority of geothermal activity and exploration is concentrated (Fleischmann, 2006). Specifically, FOH-3D was drilled in the Carson Lake field, which is structurally one of the largest basins in the Nevada Basin and Range (Carson Lake Geothermal Exploration Project, 2008; McLachlan et al., 2011). This area is comprised of inter-bedded meta-volcanic rocks, sandy sediments and stream sediments (Carson lake Geothermal Exploration Project, 2008). Recent GPS studies document an average ~1 mm/yr of active WNW-ESE extension that transitions into right later strike slip offset in northern extent of the Walker Lane Shear zone to the west (Faulds et al., 2006; Hammond and Thatcher, 2007), but with local variation in displacement direction (Hammond et al., 2007; Blewitt et al., 2009; Kreemer, et al., 2010). The mountain ranges near the studied borehole are comprised of Tertiary age rock primarily uplifted by Pleistocene fault slip (Carson lake Geothermal Exploration Project, 2008). FOH-3D was drilled through Tertiary basalts and volcaniclastic tuffs with mafic flows (Carson lake Geothermal Exploration Project, 2008). This region is part of the Central Nevada Seismic Zone and adjacent to the recent Rainbow Mountain-Fairview Peak-Dixie Valley earthquake sequence of 1954, which produced earthquake magnitudes of 6.6 to 7.2 (Hodgkinson et al., 1996). The nearby Dixie Valley geothermal system is located in the gap between these two events (Hickman et al., 2000).

Prior to the drilling of the FOH-3D borehole, two other boreholes were drilled, FOH-1 and FOH-2. FOH-1 was drilled to a depth of 617 meters, penetrating mostly unconsolidated and volcanic sediment and revealed a thermal gradient of 140°C/km (Katzenstein and Bjornstad, 1987). FOH-2 was drilled to a depth of 1367 meters, penetrating lake, stream and channel sediments deposited on top of olivine basalts inter-bedded with layers of basalt tuffs (Katzenstein and Bjornstad, 1987). FOH-3D was drilled August 1993 to a depth of 2134 meters, and later deepened in 2006 to a depth of 2743 meters. In 2006, an FMI image log was acquired from a measured depth of 1970-2730 meters as well as a BHTV log from a measured depth of 1966-2721 meters. The maximum temperature in the borehole exceeds 150ºC and has a temperature gradient of 80°C/km. More recent exploration in the Fallon area has found a range of shallow high temperatures continuing to suggest promise for this geothermal prospect (Lazaro et al., 2011; Skord, J. et al., 2011).

IMAGE LOG

Image Log Analysis Methods

Images of the borehole wall from FOH-3D produced by either measurements of electrical resistivity or acoustic reflections were analyzed to identify natural fractures, foliation and borehole deformation caused by the in-situ stress in the volume pierced by the borehole. Geophysical tools used in this study to collect the image logs were Schlumberger's Hot Hole Formation Micro Scanner (FMS), which measures the resistivity of the borehole wall within ~2.5 cm through pads of electrode arrays at a constant electrical potential pressed against the borehole wall (Ekstrom et al., 1987) and ALT's ABI85 Borehole Televiewer, which collects both the two way travel time and the amplitude of an acoustic pulse from the imaging tool reflected by the borehole wall (Zemaneck et al., 1970). Natural fractures and borehole failure structures typically appear as regions of enhanced conductivity primarily due to increased brine-filled porosity in the few centimeters of rock adjacent to the borehole in FMS logs and regions of low amplitude due to scatter of the acoustic pulse due to associated surface roughness in Televiewer logs (Figure 2). The differences in the geophysical properties measured lead to slight differences in the population of structures revealed in each log, in part because healed fractures might retain distinct porosity, but provide a relatively smooth borehole surface (see discussion in Davatzes and Hickman, 2010).

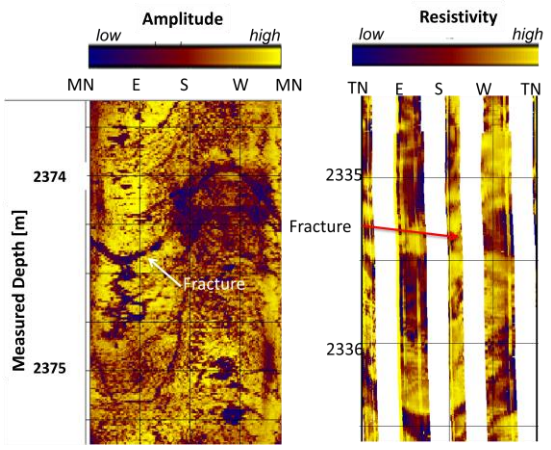

Figure 2: Sinusoidal trace of natural fractures identified in both the BHTV (left) and FMS (right) images. Natural fractures appear on the borehole well as sinusoids and in both cases appear dark in color (low amplitude or low resistivity respectively).

Along with natural fractures and foliation identified in both electrical and acoustic data, three types of drilling-induced structures were also identified in this study: breakouts, tensile fractures, and petal-centerline fractures. Failure of the borehole wall records the local orientation of the remote principal stresses (Figure 3) (Zoback et al., 1985; Barton et al., 1998; Shamir and Zoback, 1992; Barton et al., 1997; Barton and Zoback, 2002). Breakouts and tensile fractures result from the concentration of normal stress acting tangentially to the borehole wall that enhances compression or can achieve tension respectively. These structures are symmetrically distributed about the borehole. Breakouts are identified as patches of decreased acoustic amplitude, with dog-ear cross-sections and irregular edges. Tensile fractures appear as linear, paired low resistivity or acoustic amplitude features. In contrast, petal-centerline fractures form below the drill bit as the borehole is being drilled due to concentration of stress that induces tension tangential to the borehole floor (Li and Schmidt, 1999; Davatzes and Hickman, 2010; Garza-Cruz and Davatzes, 2010).

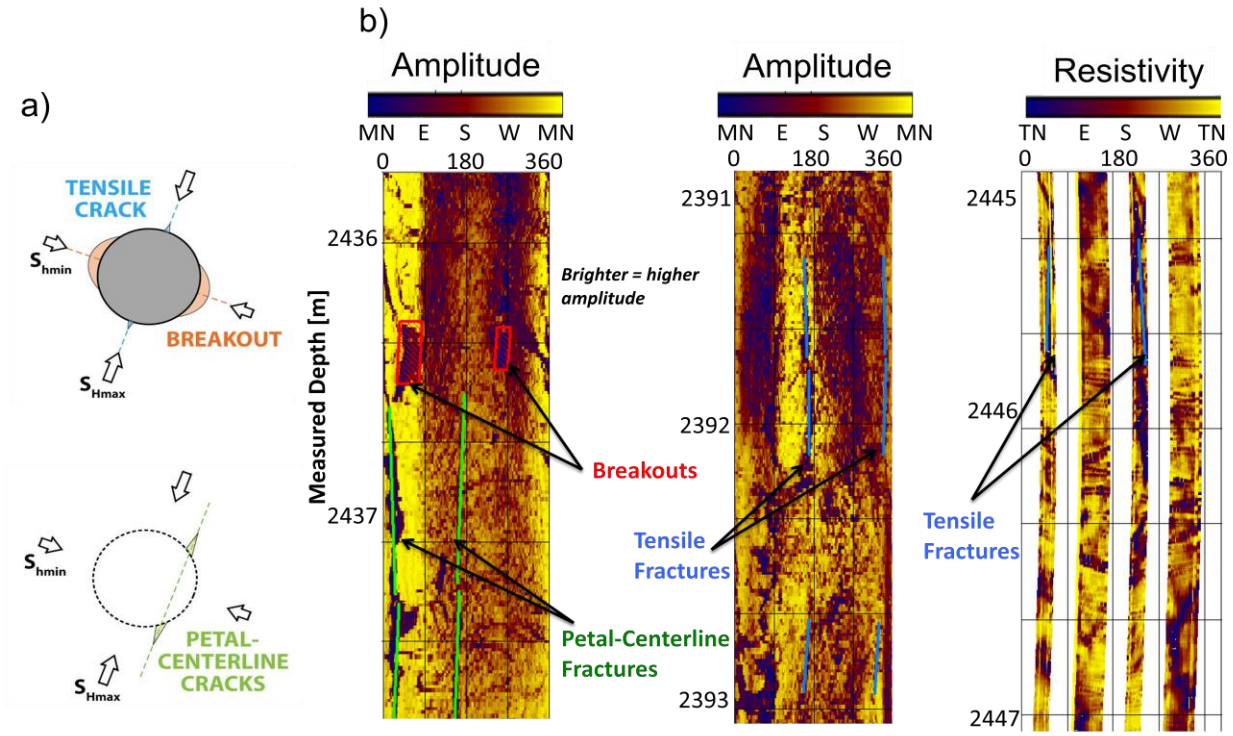

Figure 3: (a) The orientation of the borehole induced structures to the principal stress directions in a near-vertical borehole aligned with a vertical principal stress. (b) Example BHTV and FMI image logs from the Fallon FOH-3D borehole showing the mapped induced structures.

In boreholes generally 1-5 km in depth, it is reasonable to assume one principal stress is vertical consistent with Andersonian tectonics. If the borehole deviates less than 12°-15° from this stress direction, then the azimuth of breakouts corresponds to the azimuth of S_{hmin}, the azimuth of tensile fractures to S_{Hmax} (Peska and Zoback, 1995), and the average of petal centerline fractures to the azimuth of S_{hmin} (Davatzes and Hickman, 2010; Garza-Cruz and Davatzes, 2010 and references therein). In cases where the borehole deviates greater than this 12°-15°, the tangential stress on the wall of the borehole is a function of the stress directions and their relative magnitudes as all of the principal stresses contribute to the tangential normal stress. Thus, it difficult to infer the azimuth of S_{Hmax} without detailed knowledge of the principal stress magnitudes, in particular the minimum horizontal compressive principal stress, S_{hmin}. Fortunately in such cases, drilling-induced tensile fractures appear in en echelon sets, whereas in boreholes aligned with a principal stress, they are oriented parallel to the axis (see discussion in Barton and Zoback, 2002; Zoback et al., 2003). In the near-vertical section of FOH-3D, tensile fractures are oriented parallel to the borehole axis, indicating its approximate coincidence with the vertical principal stress. Consequently, we restrict our analysis to these near-vertical segments of the borehole, corresponding to measured depths greater than approximately 2316 m.

The program WellCAD was used to analyze the image logs. WellCAD provides interactive interpretation tools to identify, record, and compile the distribution and geometrical attributes of natural fractures and foliation as well as induced borehole structures. The statistical attributes of these populations were then analyzed using custom Matlab scripts. The attributes characterizing natural fractures and foliation are the measured and true vertical depth, the apparent and true dip and dip azimuth, the type of structure, and the quality of the pick. The attributes recorded for the borehole-induced structures include the measured and true vertical depth, azimuth, angular width, the height (or length) of the structure, the type of drilling-induced structure (breakout, BO; tensile fracture, TC; petal-centerline fracture, PCF) and the quality.

The quality ranking and identification criterion used in this study is taken from Davatzes and Hickman (2006; 2010) and was also used in Blake and Davatzes (2011). The drilling-induced structures were ranked in quality from '1' to '3' to distinguish the relative uncertainty of the measurement, where 1 has the lowest uncertainty. This variation in quality is summarized in Table 1.

Table 1: Quality criteria for drilling-induced structures identified.

Quality		1	2	3
FMS	Petal-Centerline	Clear image; Pair with Petal Structure (Not ~180˚ apart)	Blurry image; Pair without Petal Structure (Not ~180˚ apart)	Very blurry imag; Two structures not completely on the image log without Petal Structure (Not ~180˚ apart)
	Tensile Fractures	Clear image; Two thin vertical structures ~180˚ apart	Blurry image; Two thin vertical structures ~180˚ apart	Very blurry image; Two thin vertical structures not completely on the image log
BHTV	Petal-Centerline	Clear image; Pair with Petal Structure (Not ~180˚ apart)	Blurry image; Pair with Petal Structures (Not ~180˚ apart)	Very blurry image; Pair with Petal Structure (Not ~180˚ apart)
	Tensile Fractures	Clear image; Two thin vertical structures ~180˚ apart	Blurry image; Two thin vertical structures ~180˚ apart	Very blurry image; Two thin vertical structures ~180˚ apart
	Breakouts	Clear image; Two irregularly spaced vertical structures ~180˚ apart	Blurry image; Two irregularly spaced vertical structures ~180˚ apart	Very blurry image; Two irregularly spaced vertical structures ~180˚ apart

The FMS data spans a measured depth of 1970-2730 m and the BHTV data spans 2121-2728 m, providing considerable overlap among the two logs allowing a joint interpretation of the two image logs. A key difference we exploit is the ability of the FMS to image the distinct porosity retained in even sealed natural fractures and foliations that produce relatively little corresponding reduction in the borehole acoustic amplitude image because of their minor impact on borehole surface roughness. Another difference is the lack of complete borehole coverage in the FMS log preventing appropriate characterization of breakouts, whereas the BHTV successfully reveals these structures (Figure 4).

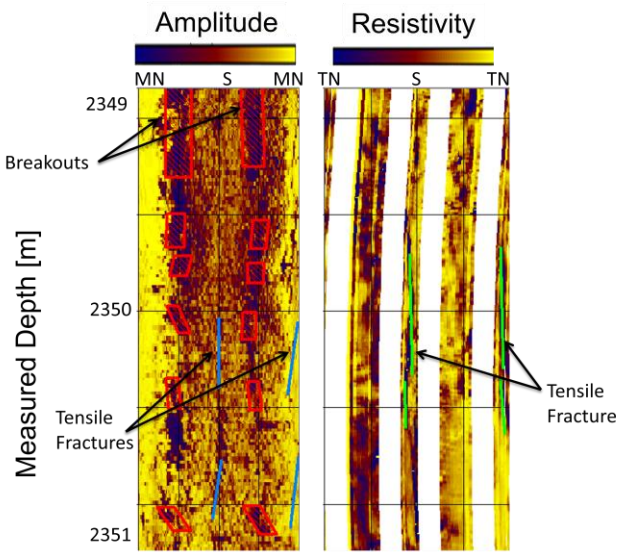

Figure 4: BHTV (left) and FMS (right) image logs of induced structures at the same depth interval demonstrate that tensile fractures can be identified in both, but breakouts are not as readily identified in the FMS data set, nor can the breakout width be quantified. In cases lacking BHTV images, the FMS image in conjunction with the caliper data is typically used identify the occurrence of breakouts following the method of Plumb and Hickman (1985).

Natural fracture population

Overall, the FMS image reveals a large number of fractures as well as extensive planar layering including foliations and flow boundaries, whereas, the BHTV image shows fewer of each. Both logs show comparable fracture attitudes, although the FMI indicates a wider range of fracture strikes compared to BHTV (Figure 5). In the BHTV log in particular, a large proportion of the identified fractures fall into a conjugate set which strikes ~010° and dips at ~58° to the E and W (Figure 5a), similar to the strike of the Stillwater Range Front Fault to the west of the studied borehole, as well as numerous faults in the Carson Sink (Caskey et al., 2004). These fracture sets occur throughout the imaged depth-interval. These natural fractures cut across foliations in the BHTV, which on average strike 009° and dip at 56° to the E (Figure 5b). Natural fractures in the FMS are characterized by an average strike of 025° due to greater variability and dips 50-75°, averaging 58° to the E and W and the average foliation strikes 020° and dips 58° (Figure 5c and 5d respectively). To further characterize the foliation identified in these image logs, a gap in the BHTV foliation occurs from ~2286 to ~2347 meters, which coincides with the depth range of crystalline volcanic rock recorded in the mudlog (Figure 5b). This crystalline rock would likely make it more difficult to identify foliation in BHTV due to lower variation in rock, whereas, this gap is not represented in FMS.

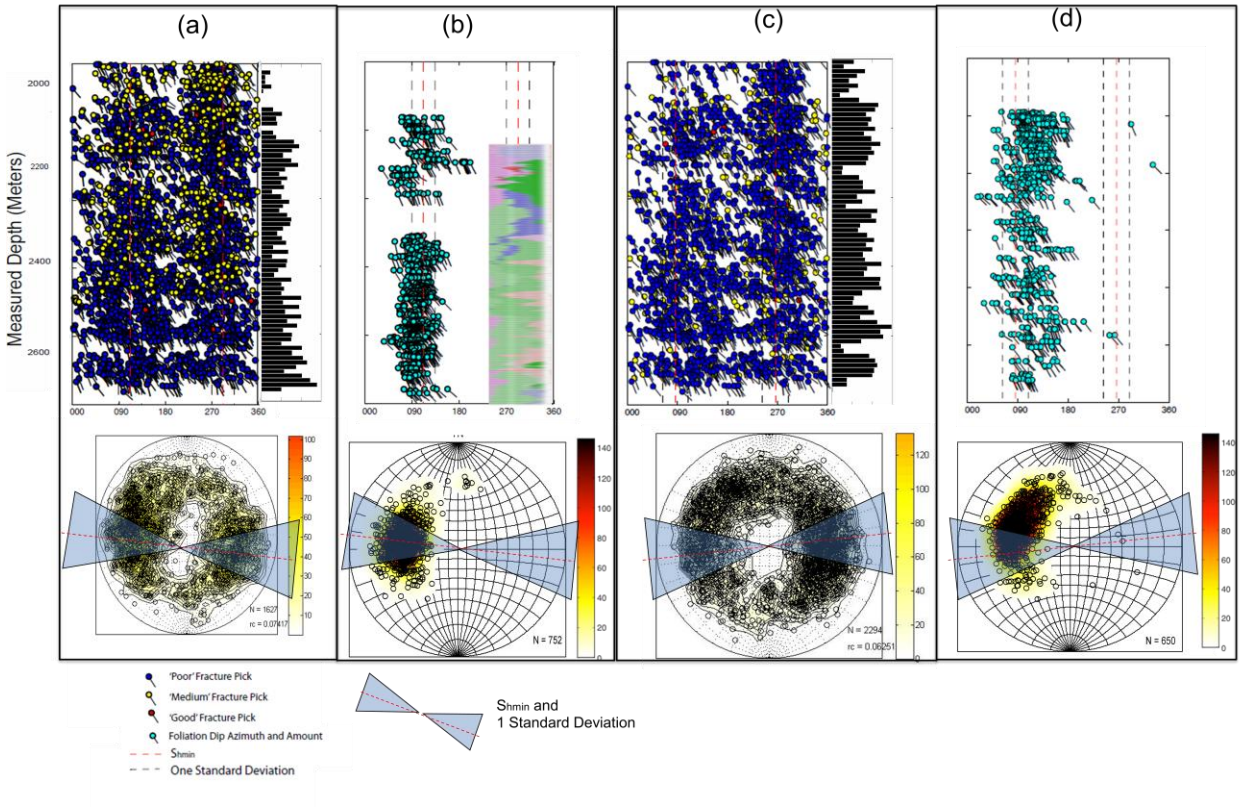

Figure 5: Summary of BHTV (a) natural fractures and (b) layering/foliation with inset lithology log, and FMS (c) natural fractures, and (d) layering/foliation. The first row presents the data as a modified tadpole plot, with azimuth on the x-axis and the tadpole indicating dip relative to horizontal and following the right-hand-rule (where dip azimuth equals the strike azimuth plus ninety degrees). The histograms to the right of the natural fracture tadpole plots are the distribution of fractures with depth. The inset lithology log (panel b) demonstrates the correlation between the crystalline tuff (royal blue) and the lack of foliation imaged in the BHTV log. The second row summarizes these data as stereonets to reveal distinct structural attitudes independent of depth. The azimuth of S_{hmin} ± one standard deviation calculated from induced structures is plotted for reference (see Figure 6a for details).

Principal horizontal stress directions in FOH-3D

Both logs reveal drilling-induced borehole failure; however, whereas the BHTV image includes extensive borehole wall breakouts, tensile fractures, and petal-centerline fractures, the FMS image only unequivocally reveals a much smaller population of tensile fractures and petal-centerline fractures (Figure 6). The average azimuth of S_{hmin} ± one standard deviation for the FMS data set is 086±16° and the BHTV is 097±12° for the near vertical portion of the borehole despite sampling across similar depth intervals (Figure 3 and Figure 4). Both azimuths are roughly similar to the regional S_{hmin} azimuths inferred from both geologic and moment tensor analysis of normal faulting in the Basin and Range province (Zoback et al., 1981; Zoback, 1989; Fauds et al., 2006) and to previous stress orientation analyses of borehole-induced structures at nearby Dixie Valley, NV (Barton et al., 1997; Hickman et al., 1998, 2000) and Desert Peak (Davatzes and Hickman, 2011) (Figure 1). Since the BHTV image log possesses greater azimuthal sampling, which allowed three distinct borehole failure structures to be distinguished, and reveals a larger population of induced structures, the S_{hmin} azimuth of 097±12° is deemed more reliable.

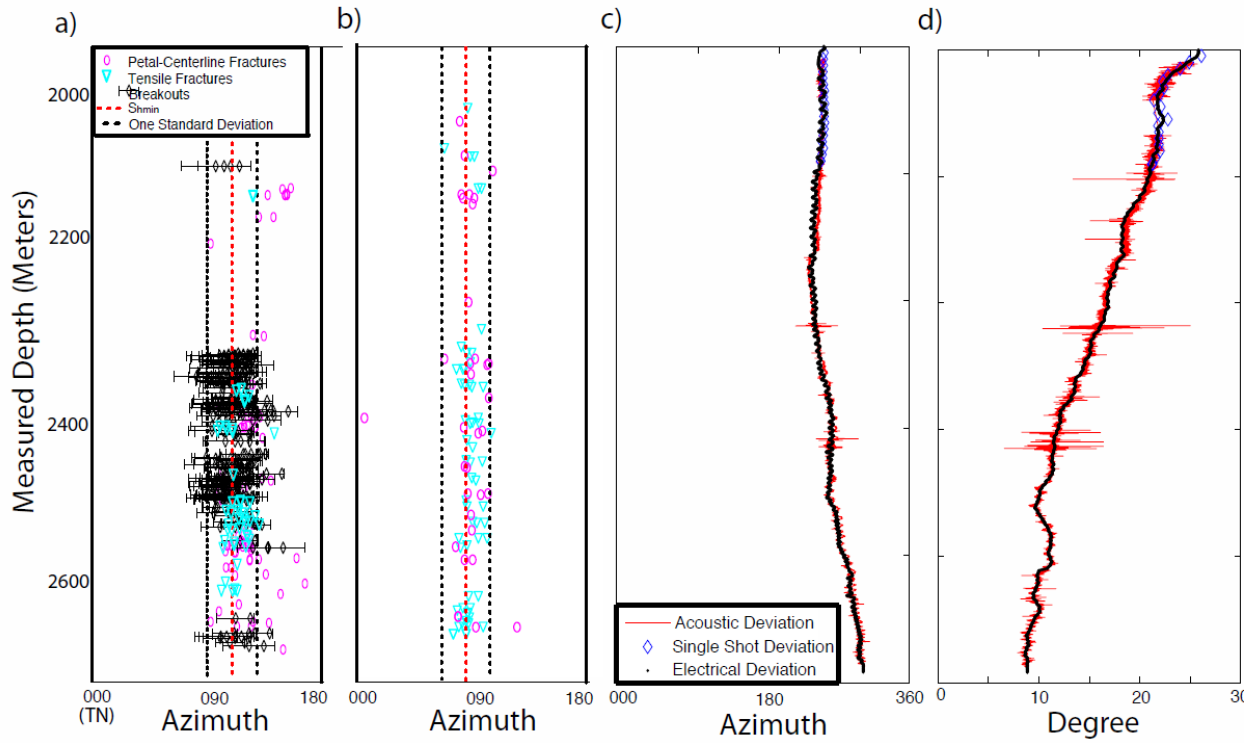

Figure 6: Average of induced structure pairs identified in the (a) BHTV, (b) FMS logs used to infer the azimuth of S_{hmin}, (c) azimuth orientation of both geophysical tools and single shot data and (d) deviation from vertical for both geophysical tools and single shot data. Only induced structures in the near vertical (deviation < 15˚ were used for principal stress calculation.

STRESS HETEROGENEITY

Spectral Analysis

The mapped variation in S_{hmin} direction varies about the mean to define a relative rotation, which can be characterized as a series of superposed sine waves with varying wavelength and amplitude. In the analysis we assume that the principal stresses primarily rotate about a vertical axis, and that each induced structure accurately samples the local direction of S_{hmin} at a particular depth along the borehole. A relative measure of how much each wavelength contributes to the distribution of stress directions is called the power spectral density, which is derived using a Fourier Transform (Hamming, 1989). The variation of the power across the wavelengths (or corresponding frequencies) determines the scaling properties of stress rotations, and thus the inherent heterogeneity of stress within the rock volume penetrated by the borehole resulting from different length-scale sources of stress perturbation from a regional mean (long-wavelength) orientation.

Previous studies, including Shamir and Zoback (1994), Day-Lewis et al. (2010), Valley and Evans (2010) and Blake and Davatzes (2011) used spectral analysis to evaluate this length-scale dependence on similar data sets of drilling-induced structures. Shamir and Zoback (1994) and Day-Lewis et al. (2010) suggest that the power is linearly distributed in log-log space and corresponds to the frequency-magnitude distribution, or b-value, of earthquakes contained in the volume traversed by the borehole. This was subsequently confirmed by Blake and Davatzes (2011) at the Coso geothermal field, who also showed that this scaling relationship was influenced by position in the geothermal field, including proximity to large faults, but did not show a clear relationship to the local production history.

A spectral analysis assumes that a data set is evenly spaced. For irregularly distributed data, the power associated with any specific wavelength of rotation (or a corresponding frequency) can be determined using one of three methods; Periodogram, Multitaper and Autoregressive Moving Average Spectral Analysis (ARMASA) (see Blake and Davatzes, 2011 and references therein). In the former methods, the field data must first be interpolated, whereas the latter method uses iterative interpolation and statistical testing in the course of the derivation of the power

spectra. Both Day Lewis et al. (2010) and Blake and Davatzes (2011) performed analyses on synthetic data sets to ensure that these analyses can be appropriately applied to measurements of stress azimuth from drilling induced structures. Blake and Davatzes (2011) discovered that the preferred spectral analysis method changed with the data set, so three different methods were applied to a synthetic data set to calculate an error estimate and determine which method provided the best results. They also estimated from comparison of synthetic colored noise of known spectral slope to the spectral slope calculated from the noise sampled at a spacing equivalent to the distribution of induced structures identified in the FOH-3D BHTV log. Once the synthetic analysis was performed, then the three methods were applied to the field data. We adopt the methods of Blake and Davatzes (2011) in the following analysis of stress heterogeneity.

Stress Heterogeneity in FOH3-D

In this analysis we focus on the BHTV stress data set due to the more complete azimuthal sampling and greater density of measurements along the borehole than revealed in the FMS images. The spacing of the data set ranges from a maximum of 112.7 m to a minimum of 0.026 m, with a mean data spacing is 2.28 m. Spectral analysis of the depth variation of the horizontal principal stress azimuth revealed in the BHTV image indicates that rotations of these stress components about the vertical axis yield a linear spectral slope (PSD) of -3.03±0.2 log (deg^2*m)(m) in a frequency range from $10^{-2.4}$ to $10^{-1.35}$ m^{-1} calculated using the ARMASA method (Figure 7). In the case of a self-affine distribution, in which anisotropic case the PSD is related to the frequency as PSD = f^{β}, where f is the frequency (m^{-1}) and β is the spectral slope (deg^2-m)(m). The lowest frequency corresponds to maximum wavelength of ~251 m, roughly one third of the depth-span of the data set, and the highest frequency corresponds to minimum detected wavelengths of ~22.4 m. This frequency range is primarily limited by the size of the sampling interval and the data spacing, and additional stress heterogeneity is expected to occur at both larger and shorter wavelengths.

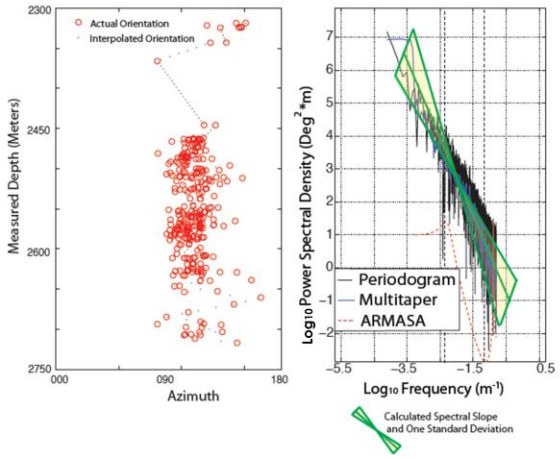

Figure7: Left: Azimuth of S_{hmin} derived from induced structure pairs in the BHTV image log with 0.5 meter data spacing interpolation in gray. Right: Power spectra derived from each of three methods, all of which yielded statistically similar spectral slopes, over a frequency range of $10^{-2.4}$ to $10^{-1.35}$ m^{-1} .

DISCUSSION

Both FMS and BHTV geophysical image logs from borehole FOH-3D drilled in volcanic and meta-volcanic rock revealed natural fractures, foliation and induced structures, however, the densities of these features varied between the two logs. This was especially evident in the number of fractures identified in FMS (2294) and BHTV (1627) (Figure 5), which demonstrates the difference in sampling between the two tools, but which may qualitatively provide information about state of fracture healing, and thus permeability of fractures proximal to this borehole. As mentioned, the fractures dip directions that appear in the BHTV image log were not as scattered as the FMS fracture dip directions (Figure 5), whereas the FMS log reveals large numbers of fractures in a variety of strike directions – although notably in both logs the dips of these fractures lie in the expected range for normal faults. One explanation for this difference is that healed fractures are often poorly imaged in BHTV logs, which only respond to the acoustic reflectivity of the borehole surfaces, but continued to be imaged by the FMS because the healed fractures retain a significant porosity contrast with the surrounding host rock. These relationships, the preferred orientation of fractures aligned to promote slip with the horizontal principal stresses and the difference in imaging response, suggest that the fractures logged in the BHTV are relatively open consistent with active deformation as proposed by Barton et al. (1995). Thus, these fracture sets are the

most likely pathway for fluid through this geothermal system.

We interpret the standard deviation of 12° in the S_{hmin} azimuth as a measure of the true heterogeneity in the stress field of the shallow crust pierced by FOH-3D (Figure 6) Such variability suggests that a range of fracture attitudes may be optimally oriented for slip, which has the practical result of aiding slip on non-coplanar fracture thus promoting connectivity and formation of an extensive facture mesh that could sustain longer-range fluid flow.

Spectral analysis of the depth variation of the horizontal principal stress azimuth along the borehole revealed in the BHTV image indicates that rotations of these stress components about the vertical axis yield a linear spectral slope of -3.03±0.2 log (deg^2*m)(m). The linear spectral slope in the resolvable frequency range is consistent with fractal behavior (Turcotte, 1997). It is also consistent with a fractal dimension that has the same scaling of power with frequency at all length scales. If we take the system to be self-affine, consistent with the progressive increase of stress magnitudes with depth and a preferred rotation around of horizontal stresses around a vertical axis as assumed in Andersonian tectonics sampled along a vertical borehole, then the fractal dimension can be derived from the power spectral slope as:

$$D_{rot} = \frac{5-\beta}{2} \qquad \text{Equation 1}$$

where β is the spectral slope calculated using stress rotations and D_{rot} is the fractal dimension of stress rotations (Turcotte, 1997). In FOH-3D, the spectral slope calculated from the rotation of the principal horizontal stress yields a fractal dimension of 0.84 to 0.98 that characterizes the heterogeneity in the stress state.

An important source of rotations in principal stress directions is recent fracture slip (e.g., as discussed by Scholz, 2002; Jaeger et al., 2007). In this case, earthquakes provide a means of sampling the potential distribution of stress rotations due to fault slip (see Day-Lewis, 2010 and arguments therein). Earthquakes demonstrate a fractal distribution relating the $\log_{10}$(frequency) of earthquake magnitudes which can be calculated as (Shamir and Zoback, 1992; Day-Lewis et al, 2010; Blake and Davatzes, 2011):

$$D_{eq} = -\frac{bd}{q} \qquad \text{Equation 2}$$

where *b* is the slope of earthquake magnitude versus log(frequency), *d* represents the shape of the fracture that slips in the earthquake and *q* is the relationship between moment magnitude and magnitude of the earthquake and D_{eq} is the fractal dimension of the earthquakes (Gutenberg and Richter, 1944; Kanamori and Anderson, 1975). Thus, both rotations of the horizontal principal stress azimuth and earthquakes demonstrate fractal relationships. If earthquakes are the principal source of the stress rotations, then these fractal dimensions should match.

The overall Basin and Range earthquake b value is 1.15, which yields an earthquake fractal dimension of 1.53 to 2.3, when *d* ranges from 2 to 3 and *q* is taken as 1.5 (Day-Lewis et al., 2010; Kanamori and Anderson, 1975). The b value for Fairview Peak-Dixie Valley earthquakes is 1.04 (Ryall and Priestley, 1975), which, when using the same variable values, yields an earthquake fractal dimension of 1.38 to 2.08. Neither of these values overlap the fractal dimension of the stress heterogeneity for the FOH-3D borehole. It is possible that this discrepancy may be due to the lack of micro seismicity sampled in both estimates of the b values.

The fractal dimension of the stress heterogeneity in FOH-3D is lower than values from Coso Geothermal Field which ranges from 1.23 to 1.55 and lower than values from the Soultz EGS reservoir, which were calculated as 1.37 and 1.55 (Blake and Davatzes, 2011; Valley and Evans, 2010). This smaller fractal dimension calculated from the FOH-3D data, and thus greater spectral slope, suggests more spectral energy is derived from lower frequency, or longer wavelength rotations, sources. If fractures are the primary source of stress heterogeneity, then this corresponds to slip on longer fractures/larger earthquake magnitudes. In the two studies where the system has been producing energy, the slope is shallower than FOH-3D, suggesting that sources of spectral energy are skewed to shorter wavelengths consistent with a preponderance of smaller earthquakes resulting from production. However, additional study of stress rotations and earthquake b-values is warranted to substantiate this potential relationship.

Together, the organization of the fracture population into conjugate sets and the relative azimuth of S_{Hmax} consistently parallel to the strike of the conjugate set indicate that these fractures are well-oriented for

normal slip. Stress heterogeneity will aid fluid movement through a geothermal system by promoting slip on a wider range fracture attitudes. The persistence of the fractal slope across the frequency range sampled indicates that slip on fractures of multiple length-scales is contributing to stress heterogeneity, suggesting a highly stress and at least moderately actively deforming fracture system. The relatively low fractal dimension at FOH-3D is also consistent with contributions to stress heterogeneity from slip on larger faults, which have the greatest potential to extend to greater depths and thus form a more persistent conduit for hot fluid to circulate to the surface. This is particularly interesting in view of the large historic earthquakes on range-bounding faults in the vicinity. However, we are not able to verify this interpretation by direct comparison to the b-value derived from earthquakes sensed by regional seismometer networks. Other sources of stress heterogeneity that bear investigation are topography and variation in the elastic properties of the rocks traversed by the borehole, which are known to produce variations in stress magnitudes (see discussions in Zoback, (2007) and Zang and Stephansson (2010)).

During stimulation, this stress heterogeneity should promote a widening of the stimulation volume, and in concert with fracture dilation accompanying slip can contribute to the porosity necessary to store the fluid and surface area necessary to exchange heat required to sustain a geothermal reservoir. However, the potential correlation between the dimensions of the stimulation volume, the natural fracture population and stress heterogeneity remains untested.

In the regional context, the stress information gained through the analysis of FOH-3D demonstrates rotations of the principal stresses at the centimeter scale to the multiple kilometer scale (Figure 1 and Figure 6). The orientation of S_{Hmax} in Dixie Valley is roughly northeast-southwest and over a span of ~50 km has rotated to north-south based on the borehole data analyzed near Brady's Hot Springs, NV. At each site, the S_{Hmax} orientation is closely tied to a fault system associated with the geothermal field, and consistent with active normal faulting as part of the transition zone between Basin and Range to Walker Lane movement.

CONCLUSION

Highly stressed volumes with fractures well-oriented to slip are considered a pre-requisite for active hydrothermal systems and candidates for EGS stimulation. The average S_{hmin} azimuth is 097±12° and the predominate strike of fractures is N-NE and S-SW with typical dips for normal faults in the BHTV log, with a wider range of fracture attitudes evident in the FMS log, but which retain typical normal faulting tips. The attitude of natural fractures and the horizontal principal stress directions are consistent with normal slip and the geometry of the basin-bounding faults, recent large earthquakes in the surrounding ranges and other similar borehole analyses. Thus, both the FMS and the BHTV logs from borehole FOH-3D drilled in Fallon, NV indicate a large density of fractures including fractures well-oriented for slip given the azimuth of S_{hmin} inferred from borehole failure. In addition, spectral analysis is used to calculate a spectral slope and fractal dimension that quantify the heterogeneity of stress as a function of length-scale in borehole FOH-3D and suggest stress heterogeneity is primarily contributed by relatively long wavelength sources.

AKNOWLEDGEMENTS

We would like to thank the Navy Geothermal Program office, specifically Steve Bjornstad and the USGS, specifically Robert Summers and Joe Svitek for providing the data for this analysis. Special thanks would also like to be given to the Davatzes Geomechanical and Geothermal Research Lab and Amy Day-Lewis for help throughout the research. Funding for this project was provided by the Navy Geothermal Program Office and Epsilon Systems Solutions.

REFERENCES

Barton, C.A., Hickman, S., Morin, R., Zoback, M.D., Finkbeiner, T., Sass, J. and Benoit, D. (1997), "Fracture Permeability and its Relationship to In-Situ Stress in the Dixie Valley, Nevada, Geothermal Reservoir," *Proceedings Twenty-Second Stanford University Geothermal Workshop*.

Barton, C.A., Castillo, D.A., Moos, D., Peska, P. and Zoback, M.D. (1998), "Characterizing the full stress tensor based on observations of drilling-induced wellbore failures in vertical and inclined boreholes leading to improved wellbore stability and permeability prediction," *APPEA Journal*, 29-53.

Barton, C.A. and Zoback, M.D. (2002), "Wellbore imaging technologies applied to reservoir geomechanics and environmental engineering," *AAPG Methods in Exploration*, **13**, 229-239.

Bellier, O. and Zoback, M.L., (1995), "Recent state

of stress change in the Walker Lane zone, western Basin and Range province, United States," *Tectonics*, **14(3)**, 564-593.

Bennett, R. A., B. P. Wernicke, N. A. Niemi, A. M. Friedrich, and J. L. Davis (2003), "Contemporary strain rates in the northern Basin and Range province from GPS data," *Tectonics*, 22(2), 1008, doi:10.1029/ 2001TC001355.

Blake, K. and Davatzes, N.C. (2011), "Crustal Stress Heterogeneity in the Vinicity of Coso Geothermal Field, CA," *Proceedings Thiry-Seventh Stanford University Geothermal Workshop.*

Blewitt, G., Hammond, W.C., and Kreemer, C. (2009), "Geodetic observation of contemporary deformation in the northern Walker Lane: 1. Semipermanent GPS strategy," *Geological Society of America Special Paper*, 1-15.

Carson Lake Geothermal Exploration Project Environmental Assessment, (2008).

Caskey, S.J., Bell, J.W., Ramelli, A.R., and Wesnousky, S.G. (2004), "Historic Surface Faulting and Paleoseismicity in the Area of the 1954 Rainbow Mountain-Stillwater Earthquake Sequence, Central Nevada," *Bulletin of the Seismological Society of America*, **94**, 1255-1275.

Curewitz, D., and J. A. Karson,(1997), "Structural settings of hydrothermal outflow: Fracture permeability maintained by fault propagation and interaction," *J. Volcanol. Geotherm. Res.*, **79**, 149–168.

Davatzes, N.C. and Hickman, S. (2006), "Stress and faulting in the Coso Geothermal Field: Update and recent results from the East Flank and Coso Wash," *Proceedings Thirty-First Stanford University Geothermal Workshop*.

Davatzes, N.C. and Hickman, S. (2009), "Stress, fracture, and fluid-flow analysis using acoustic and electrical image logs in hot fractures granites of the Coso Geothermal Field, California," *AAPG Memoir*, **92**, 1-35.

Davatzes, N.C. and Hickman,S. (2010), "The feedback between stress, faulting, and fluid flow: Lessons from the Coso Geothermal Field, CA, USA," *Proceedings World Geothermal Congress 2010*, 1-14.

Davatzes, N.C. and Hickman, S. (2011), "Natural Fractures, Mechanical Properties, and In-Situ Stress in the Planning and Execution of the Desert Peak EGS Experiment," *Proceedings AAPG/SPE/SEG Hedberg Conference*.

Day-Lewis, A., Zoback, M.D. and Hickman, S. (2010), "Scale invariant stress orientations and seismicity rates near the San Andreas Fault," *Geophysical Research Letters*, **37**, L24304, doi: 10.1029/2010FLO45025

Eaton, G.P. (1982), "The Basin and Range Province: Origin and Tectonic Signifance," *Ann. Rev. Earth and Planetary Science*, **10**, 409-440.

Ekstrom, M.P., Dahan, C, Chen, M.-Y., Lloyd, P., and Rossi, D.J., (1987), "Formation imaging with microelectrical scanning arrays," *Log Analyst*, **28**, 294-306.

Faulds, J.E., Coolbaugh, M.F., Vice, G.S., and Edwards, M.L. (2006), "Characterizing Structural Controls of Geothermal Fields in the Northwestern Great Basin: A Progress Report," *Geothermal Resources Council Transactions,* **30,** 69-76.

Fleischmann, D. (2006), "Geothermal Resource Development in Nevada-2006: Existing efforts and next steps to successful development in the Silver State," *Geothermal Energy Association*.

Garza-Cruz, T. and Davatzes, N.C. (2010), "Numerical Modeling of the Nucleation Conditions of Petal-Centerline Fractures Below a Borehole Floow, A Sensitivity Study and Application to the Coso Geothermal Field," *Geothermal Resource Council*.

Gutenberg, B., and Richter, C.F. (1944), "Frequency of earthquakes in California," *Bulletin Seismology Society of America*, **34**, 185-188.

Hamming, R. W. (1989), *Numerical Methods for Scientists and Engineers*, Dover Publications, Inc. New York, NY, p. 503-516.

Hammond, C., Kreemer, C., and Blewitt, G. (2007), "Exploring the Relationship between Geothermal Resources and Geodetically Inferred Faults Slip Rates in the Great Basin," *Geothermal Resource Council*, **31**, 391-395.

Hammond, W. and Thatcher, W. (2001), "Northwest Basin and Range tectonic deformation observed with the Global Positioning System, 1999–2003,"

Journal of Geophysical Research, **110**, 12.

Heffer, K. (2002), "Geomechanical Influences in Water Injection Projects: An Overview," *Oil and Gas Science and Technology*, **57**, 415- 422.

Heidbach, O., Tingay, M., Barth, A., Reinecker, J., Kurfeß, D. and M**ü**ller, B. (2010), "Global crustal stress pattern based on the World Stress Map database release 2008," *Tectonophysics*, **482**, 3-15.

Hickman, S., Zoback, M.D. and Benoit, R. (1998). "Tectonic controls on fault-zoine permeability in a geothermal reservoir at Dixie Valley, Nevada," *Rock Mechanics in Petroleum Engineering*, **1**, 79-86.

Hickman, S., Zoback, M.D., Barton, C., Benoit, R., Svitek, J. and Summers, R. (2000), "Stress and permeability heterogeneity within the Dixie Valley geothermal reservoir: Recent results from well 82-5," *Proceedings Stanford University Geothermal Workshop*.

Hill, D. P. (1971), "Velocity Gradients and Anelasticity from Crustal Body Wave Amplitudes," *Journal of Geophysical Research*, **76**, 3309-3325.

Hodgkinson, K.M, Stein, R.S. and King, G.C.P. (1996), "The 1954 Rainbow Mountain-Fairview Peak-Dixie Valley earthquakes: A triggered normal fault sequence," *Journal of Geophysical Research*, **101**, 25459-25471.

Jaeger, J.C., Cook, N.G. and Zimmerman, R.W. (2007), *Fundamentals of Rock Mechanics*. 4. 1. Malden, MA: Blackwell Publishing, 1-7.

Kanamori, H., and Anderson, D.L. (1975), "Theoretical basis of some empirical relations in seismology," *Bulletin Seismological Society of America*, **65**, 1073-1095.

Katzenstein, A.M. and Bjornstad, S.C. (1987), "Geothermal Resource Evaluation at Naval Air Station Fallon, Nevada," Naval Weapons Center Technical Publication 6808.

Kreemer, C., G. Blewitt, and W. C. Hammond (2009), "Geodeticon contemporary deformation in the northern Walker Lane: 2, velocity and tensor strain rate analysis," *Late Cenozoic Structure and Evolution of the Great Basin – Sierra NevadaTransition, Special Paper 447, doi: 10.1130/2009.2447(02)*.

Kreemer, C., Blewitt, G., and Hammond, W.C. (2010), "Evidence for an active shear zone in southern Nevada linking the Wasatch fault to the Eastern California shear zone," *Geology*, **38**, 475-478.

Lazaro, M., Alm, S., Tiedeman, A., Page, C., Meade, D., Shoffner, J., and Bucher, K. (2011), "Department of the Navy Geothermal Exploration on Naval Air Station Fall (NASF) Managed Lands in Dixie Valley, Nevada," *Geothermal Resource Council Transactions 2011*.

Li, Y. and Schmidt, D.R. (1999), "Well-bore bottom stress concentration and induced core fractures," *AAPG Bulletin*, **81**, 1909-1925.

Majer, E.L., Baria, R., Stark, M., Oates, S., Bommer, J., Smith, B., Asanuma, H. (2007), "Induced seismicity associated with Enhanced Geothermal Systems," *Geothermics*, **36**, 185–222

McLachlan, H., Benoit, W., and Faulds, J. (2011), "Structural Framework of the Soda Lake Geothermal Area, Churchill County, Nevada," *Geothermal Resource Council Transactions 2011*.

Peska, P. and Zoback, M.D. (1995), "Compressive and tensile failure of inclined well bores and determination of in situ stress and rock strength," *Journal of Geophysical Research*, **100**, 27911-12811.

Plumb RA, Hickman SH. (1985). Stress-induced borehole elongation: a comparison between the four-arm dipmeter and the borehole televiewer in the auburn geothermal well. *Journal of Geophysical Research*, **90**, 5513–5521.

Robertson-Tait, A., Lutz, S.J., Sheridan, J., and Morris, C.L. (2004), "Selection of an interval for massive hydraulic stimulation in well DP 23-1, Desert Peak East EGS project, Nevada," *Proceedings, Twenty-Ninth Workshop on Geothermal Reservoir Engineering*.

Rutledge, J.T., W.S. Phillips, M.J. Mayerhofer (2004), "Faulting Induced by Forced Fluid Injection and Fluid Flow Forced by Faulting: An Interpretation of Hydraulic-Fracture Microseismicity, Carthage

Cotton Valley Gas Field, Texas," *Bulletin of the Seismological Society of America*, **94**, 1817-1830.

Ryall, A and Priestley, K (1975), "Seismicity, Secular Strain, and Maximum Magnitude in Excelsior Mountains Area, Western Nevada and Eastern California," *Geological Society of America Bulletin*, **86**, 1585-1592.

Scholz, C. (2002), *The Mechanics of Earthquakes and Faulting*, 2. 1. New York, NY: Cambridge, p. 174-243.

Shamir, G., and Zoback, M.D. (1992), "Stress orientation profile to 3.5 km depth near the San Andreas fault at Cajon Pass, Californi,": *Journal of Geophysical Research*, **97**, 5059-5080.

Skord, J., Sladek, C., Coolbaugh, M, Cashman, P., Lazaro, M., and Kratt, C. (2011), "Two-Meter Temperature Surveys for Geothermal Exploration Project at NAS Fallon," *Geothermal Resource Council Transactions 2011*.

Thatcher, W., G.R. Foulger, B.R. Julian, J. Svarc, E. Quilty, G.W. Bawden (1999) Present-Day Deformation Across the Basin and Range Province, Western United States, Science, v. 283, p. 1714-1718.

Turcotte, D.L. (1997), *Fractals and Chaos in Geology and Geophysics*, 2.1. New York, NY: Cambridge, pg. 56-79.

Valley, B. and Evans, K.R. (2010), "Stress Heterogeneity in the Granite of the Soultz EGS Reservoir Inferred from Analysis of Wellbore Failure," *Proceedings World Geothermal Congress 2010*, Bali, Indonesia.

World Stress Map (2008), http://www.world-stress-map.org.

Zhang, A, and O. Stephansson. (2010). Stress Field of the Earth's Crust, Springer, New York, 322.

Zemanek, J., Caldwell, R.L., Glenn, E.E., Holcomb, S.V., Norton, L.J., and Strauss, A.J.D., (1970), "The borehole televiewer—a new logging concept for fracture location and other borehole inspection," *Journal Petrographic Techtonics*, **21**, 762-774.

Zoback, M.D., and Zoback, M.L. (1981), "State of stress and intraplate earthquakes in the United States," *Science*, **231**, 96-104.

Zoback, M.D., Moos, D., Mastin, L. and Anderson, R.N. (1985), "Wellbore breakouts and in-situ stress, Journal of Geophysical Research," **90**, 5,523-5,530.

Zoback, M.L., Zoback, M.D., Adams, J., Assumpcão, M., Bell, S., Bergman, E.A., Blümling, P., Brereton, N.R., Denham, D., Ding, J., Fuchs, K., Gay, N., Gregersen, S., Gupta, H.K., Gvishiani, A., Jacov, K., Klein, R., Knoll, P., Magee, M., Mercier, J.L., Müller, B.C., Paquin, C., Rajendran, K., Stephansson, O., Suarez, G., Suter, M., Udias, A., Xu, Z. H. and Zhizhin, M. (1989), "Global patterns of tectonic stress," *Nature*, **341**, 291-298.

Zoback, M.L. (1989), "State of Stress and Modern Deformation of the Northern Basin and Range Province," *Journal of Geophysical Research*, **94(B6)**, 7105-7128.